

Chapter 2

Effect of SHN on the Phase Behaviour of Some Cationic Surfactants

2.1 Introduction

The physical properties of ionic surfactants are very sensitive to the nature of the counterions. In particular, counterions that have a tendency to adsorb on the surfactant micelle are known to dramatically modify the viscoelastic properties of these solutions through the formation of long worm-like micelles [1, 2, 3, 4]. One extreme limit of an adsorbed counterion is an oppositely charged surfactant, and aqueous solutions of such surfactant mixtures are known to show interesting properties, such as low critical micellar concentration (CMC), high surface activity, formation of liquid crystalline phases at higher water content and spontaneous formation of vesicles [5, 6, 7, 8, 9].

This chapter deals with the effect of the strongly bound hydroxy naphthoate (HN^-) counterion on the phase behaviour of concentrated aqueous solutions of three cationic surfactants, namely, cetyltrimethylammonium bromide (CTAB), cetyltrimethylammonium chloride (CTAC) and dodecyltrimethylammonium bromide (DTAB). This counterion is introduced by adding 3-sodium-2-hydroxy naphthoate (SHN) to the surfactant solution. Earlier studies on similar systems are described in section 2.2. In section 2.3, a brief description of the experimental techniques used in these studies has been given. Our results are described in section 2.4. At low amounts of SHN, the phase behavior of CTAB-SHN-water system is similar to that of the CTAB-water binary system, which exhibits a hexagonal (H_I) phase over a wide range of water content. With increasing SHN concentration a lamellar phase with curvature defects is found instead of the H_I phase. At

lower temperatures ($< \sim 60$ °C) this phase transforms into a regular lamellar phase via an intermediate phase on decreasing the water content. At still higher SHN concentration a nematic phase is found. A partial ternary phase diagram has been constructed, which exhibits a high degree of symmetry about the equimolar CTAB/SHN composition, reminiscent of the phase behavior of mixtures of anionic and cationic surfactants. On replacing the bromide (Br^-) counterion of the surfactant by chloride (Cl^-), the CTAC-SHN-water system shows only a regular lamellar phase around the equimolar composition. Decreasing the chain length of the surfactant, the DTAB-SHN system forms the lamellar phase with curvature defects but the intermediate phase is not observed in this system. A detailed discussion of our results is given in section 2.5, and the conclusions that can be drawn from this study are given in section 2.6.

2.2 Earlier studies

The CTAB-water binary system forms an isotropic solution of spherical micelles just above the CMC. On increasing the surfactant concentration the micelles become rod-like. With further addition of surfactant a nematic phase made up of rod-like micelles is observed below 42°C over a narrow concentration range (26 - 30 wt%), beyond which a 2D hexagonal phase is seen [10, 11]. Addition of organic salts, such as sodium salicylate (SS), transforms the rod-like CTAB micelles into long worm-like micelles, whose rheological properties have been the subject of many theoretical and experimental studies [3, 4]. A somewhat similar system that has been well studied are mixtures of CTAB with sodium hydroxy naphthoate (SHN), which also exhibits a shear-induced vesicle to micelle transition [12, 13, 14, 15, 16]. However, all these investigations have been confined to dilute solutions with surfactant concentrations ≤ 5 wt%. At much higher concentrations a number of liquid crystalline phases have been reported recently for a few surfactant compositions with the SHN to CTAB molar ratio less than 1.0, and an intermediate phase was observed between the hexagonal and lamellar phases, which was tentatively identified as a rectangular phase [17] (Fig. 2.1). Here we extend these investigations to higher SHN to CTAB molar ratios and characterize the observed phases in detail using optical microscopy and x-ray diffraction.

The phase behaviour of the CTAC-water system is similar to that of the CTAB-water system,

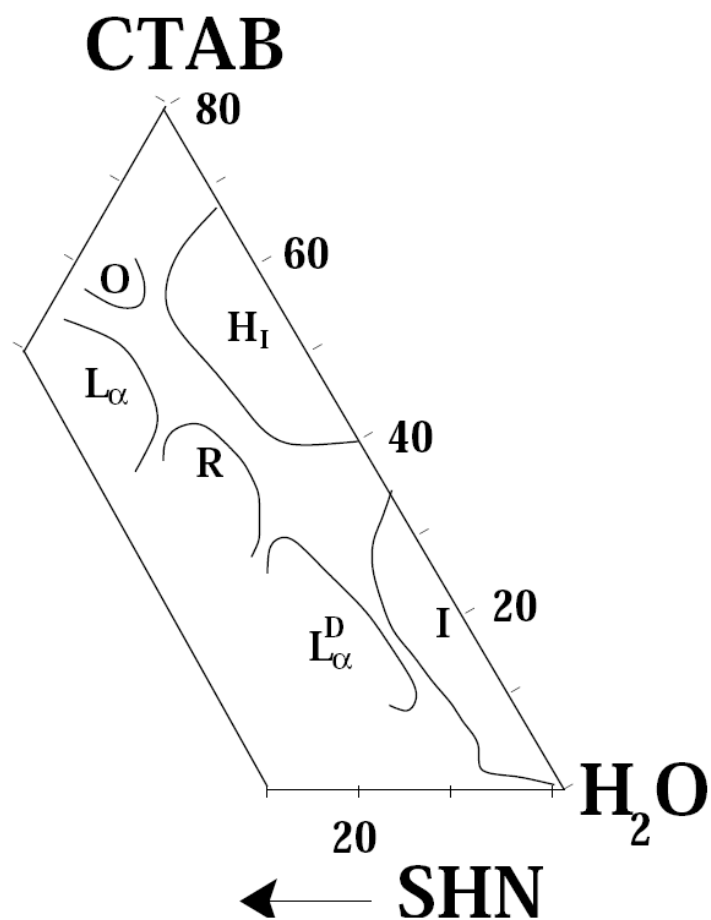


Figure 2.1: Partial phase diagram indicating the various liquid crystalline phases of CTAB-SHN-water system at 30 °C. I , L_{α}^D , R , H_I , O and L_{α} denote the isotropic, lamellar with curvature defects, centred rectangular, 2D hexagonal, 2D oblique and regular lamellar phases, respectively [17].

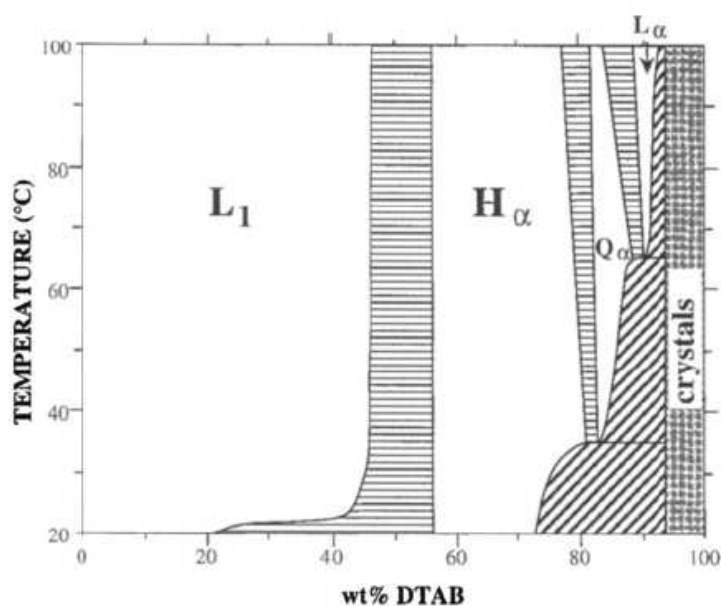


Figure 2.2: Partial phase diagram indicating the various liquid crystalline phases of DTAB-water system at 30 °C. L_1 , H_α , Q_α and L_α denote the isotropic, hexagonal, cubic and lamellar phases, respectively [19].

except for the appearance of cubic phases between the hexagonal and lamellar phases. In the bicontinuous cubic phases observed here between 75 to 83 wt% surfactant concentration, the surfactant molecules are reported to be arranged on minimal surfaces, which have vanishing mean curvature at every point [18].

At very low surfactant concentration, the DTAB-water binary system also exhibits an isotropic solution of spherical micelles. With further addition of the surfactant, it first forms a hexagonal phase and then a lamellar phase at very high concentration (> 85 wt%). Between the hexagonal and lamellar phases there is a narrow concentration range over which a bicontinuous cubic phase is observed (Fig. 2.2) [19]. Addition of the anionic surfactant sodium dodecylsulfate (SDS) to DTAB leads to spontaneous formation of unilamellar vesicles, made up of single bilayers. At low water content, this system shows a symmetric phase diagram about the equimolar line [8].

2.3 Experimental

All the surfactants and 3-hydroxy-2-naphthoic acid (HNA) were purchased from Aldrich. Sodium-3-hydroxy-2-naphthoate (SHN) was prepared by adding equivalent amount of an aqueous solu-

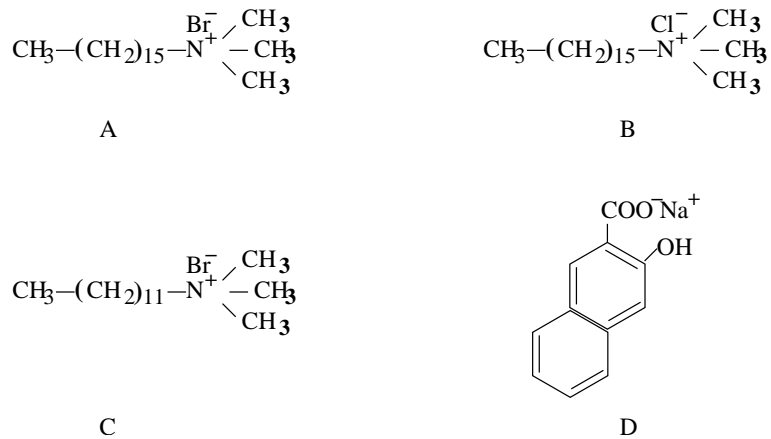


Figure 2.3: Chemical structure of (A) cetyltrimethylammonium bromide (CTAB), (B) cetyltrimethylammonium chloride (CTAC), (C) dodecyltrimethylammonium bromide (DTAB) and (D) 3-sodium-2-hydroxy naphthoate (SHN).

tion of sodium hydroxide (NaOH) to an ethanol solution of HNA. The chemical structures of the molecules are shown in figure 2.3. To prepare the ternary solution, appropriate amounts of the surfactant and SHN were first weighed out into a tube. The required concentration of the surfactant solution was obtained by adding de-ionized water. The tube was then sealed and left in an oven at 40°C for more than two weeks. For microscopic observations the samples were taken in between a glass slide and a cover slip. Samples were taken in glass capillaries for x-ray diffraction studies. Aligned samples in the lamellar phase were obtained by sucking them into thin capillaries of 0.5 mm diameter. One mm diameter capillaries were used to obtain unoriented samples. The capillaries were flame-sealed, and the sealed ends were dipped in glue as an additional precaution against loss of water from the sample. A rotating anode generator (Rigaku, UltraX 18) operating at 48 kV and 80 mA was the source of x-rays. Cu K_{α} radiation (0.154 nm) was selected by using a flat graphite monochromator (Huber). Diffraction patterns were collected on an image plate detector (Marresearch). Typical exposure time was one to two hours.

2.4 Results

2.4.1 CTAB-SHN-water system

The phase behaviour of mixtures of CTAB and SHN was studied at different values of their molar ratio ($\alpha = \frac{[SHN]}{[CTAB]}$). For each α the total concentration ($\phi_s = \frac{(CTAB+SHN)}{(CTAB+SHN+water)} \times 100\%$) was varied

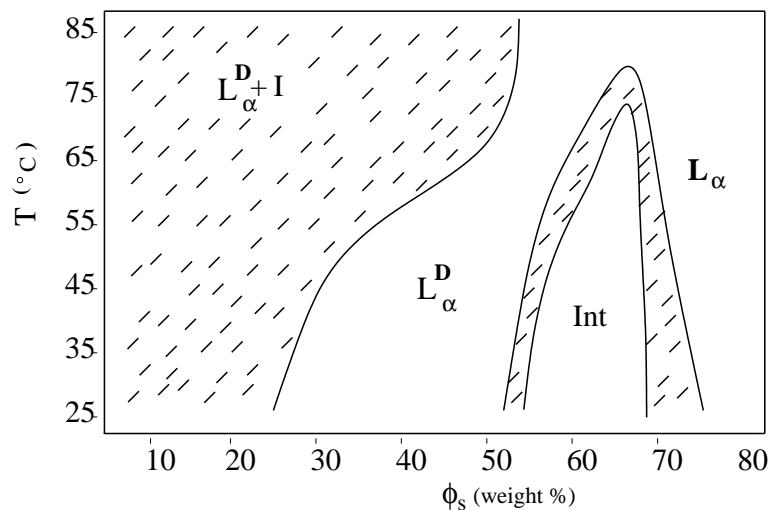


Figure 2.4: Phase diagram of the CTAB-SHN-water system at $\alpha = 1.0$. I , L_α^D , Int and L_α denote the isotropic, lamellar with curvature defects, intermediate and regular lamellar phases, respectively.

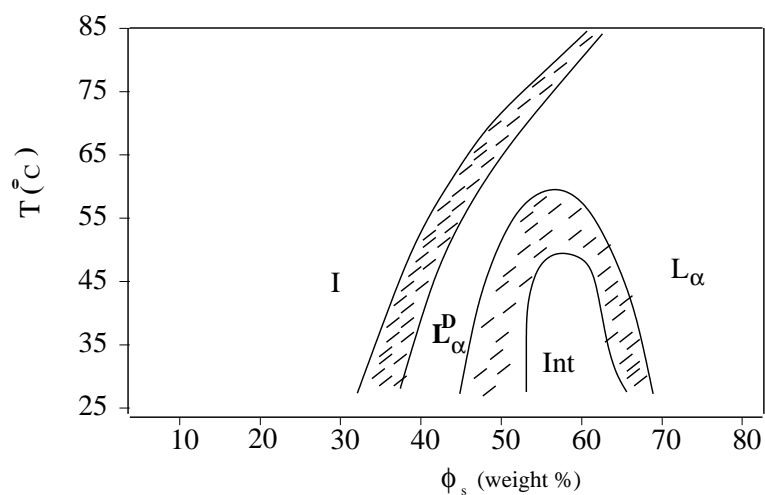


Figure 2.5: Phase diagram of the CTAB-SHN-water system at $\alpha = 1.5$.

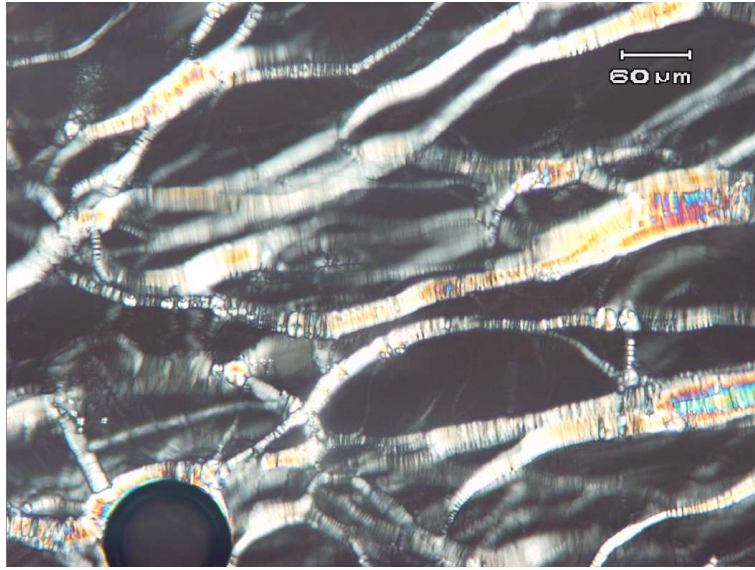


Figure 2.6: Typical oily streak texture of the lamellar phase under crossed polarizer at $\alpha = 1.5$, $\phi_s = 45$ and $T = 30$ °C.

from 10 to 80 wt%. Microscopy observations were made over a temperature range from 30 to 85 °C. Phases were identified from their characteristic microscopy textures and diffraction patterns. Multiphase regions in the phase diagrams were deduced from coexisting microscopy textures.

The phase diagram for $\alpha = 1.0$ is shown in figure 2.4. A lamellar phase is found to coexist with an isotropic phase (I) at $\phi_s = 10$. The diffraction pattern of this lamellar phase shows a diffuse peak in addition to the peaks arising from the lamellar periodicity. Such diffuse peaks have been seen in some earlier studies, and have been ascribed to curvature defects (slits or pores) in the bilayer. Hence we denote this phase as L_α^D . At higher concentrations a pure L_α^D is obtained. On increasing ϕ_s further the intermediate phase (Int) is obtained, which transforms into L_α^D on heating. At still higher ϕ_s a regular lamellar (L_α) phase appears, whose diffraction patterns do not show any evidence for defects in the bilayers. The phase behaviour for $\alpha = 1.5$ is similar to $\alpha = 1.0$ except for the appearance of a pure isotropic phase at low ϕ_s . The L_α^D phase transforms to an isotropic phase on increasing the temperature. The corresponding transition temperature increases strongly with increasing ϕ_s (Fig. 2.5).

The microscopy textures of the lamellar phase occurring on either side of Int phase at room temperature are identical (Fig. 2.6). However, as mentioned above, their diffraction patterns differ in one respect. The diffraction pattern of the L_α^D phase present at lower ϕ_s consists of two reflections

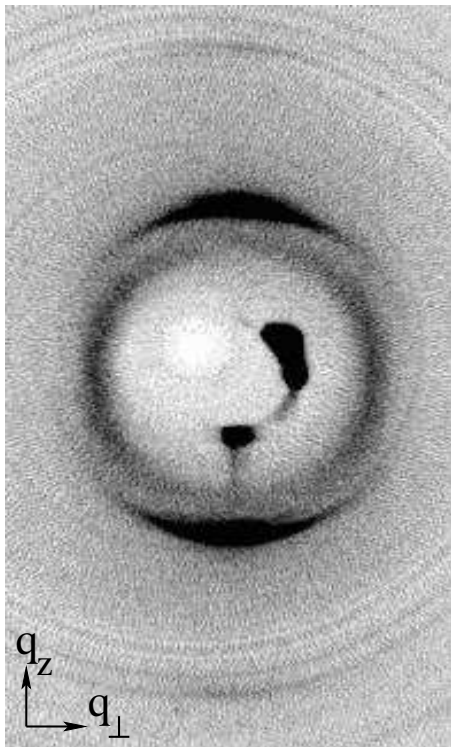


Figure 2.7: Typical diffraction pattern of the lamellar phase with curvature defects (L_α^D) at $\alpha = 1.5$, $\phi_s = 45$ and $T = 30$ °C. The irregular “spots” near the centre are due to the direct beam escaping the beam stop.

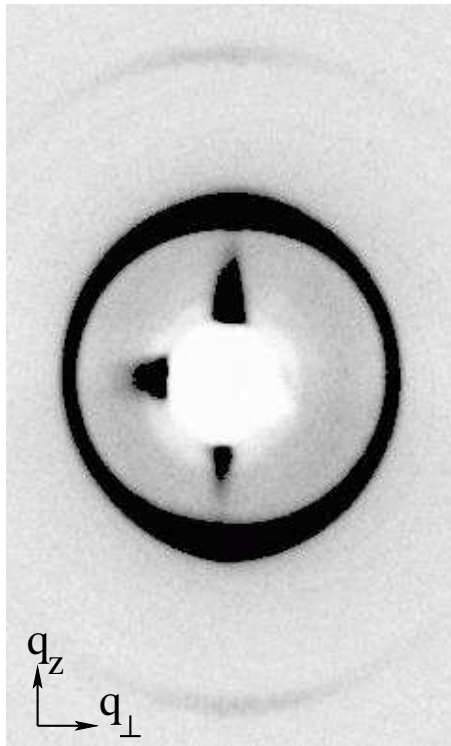


Figure 2.8: Typical diffraction pattern of the lamellar phase (L_α) occurring at very high values of ϕ_s at room temperature ($\alpha = 1.5$, $\phi_s = 80$).

corresponding to the lamellar periodicity along q_z , z being the direction of the bilayer normal, and a more diffuse reflection along the orthogonal direction q_\perp (Fig. 2.7). The diffuse reflection is absent in the L_α phase occurring at higher ϕ_s (Fig. 2.8). The lamellar periodicity and the position of the diffuse peak in the lamellar phase at $\alpha = 1.0$ are given in table 2.1 as a function of ϕ_s . At high temperatures the diffuse peaks fade away gradually on increasing ϕ_s . On the other hand, at lower temperatures the *Int* phase intervenes between the two lamellar structures. This is the reason for referring to this as the intermediate phase. The texture of this phase is different from that of the other liquid crystalline phases (Fig. 2.9). The phase is found to be much more viscous than the other phases observed in this system at similar surfactant concentrations. Diffraction pattern of this structure contains many reflections, indicating a high degree of positional order (Fig. 2.10). It does not show any changes even after aging the samples for about 1 year, suggesting the thermodynamic stability of this phase.

At much higher SHN concentrations, the L_α phase disappears. A viscous isotropic phase is obtained at $\alpha = 1.85$ for $\phi_s \leq 30$, beyond which a nematic (N) phase appears (Fig. 2.11). The latter

ϕ_s	$d(\text{nm})$	$d_d(\text{nm})$	phase
10	4.71	-	L_α^D
20	5.37	-	L_α^D
25	6.17	-	L_α^D
30	9.60	5.94	L_α^D
40	7.17	6.93	L_α^D
50	5.85	7.45	L_α^D
80	39.8	-	L_α

Table 2.1: Variation of the lamellar periodicity d and the spacing of the diffuse peak d_d with ϕ_s at $\alpha = 1.0$ and $T = 30^\circ\text{C}$.

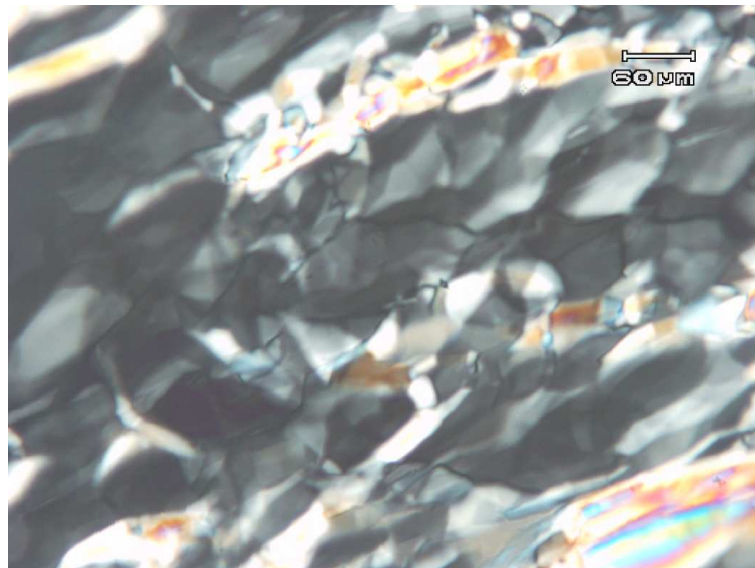


Figure 2.9: Typical mosaic texture of intermediate phase observed under crossed polarizers at $\alpha = 1.0$, $\phi_s = 60$ and $T = 30^\circ\text{C}$.

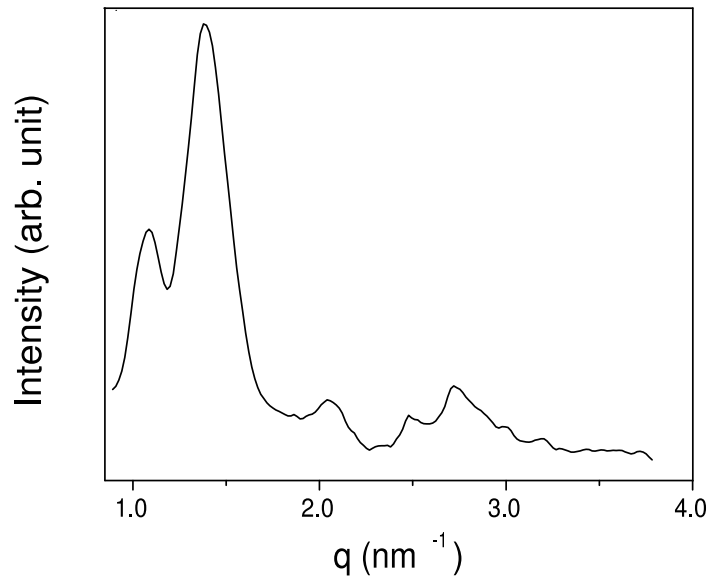


Figure 2.10: Typical diffraction pattern of the intermediate phase (*Int*) at $\alpha = 1.0$ and $\phi_s = 60$ [17].

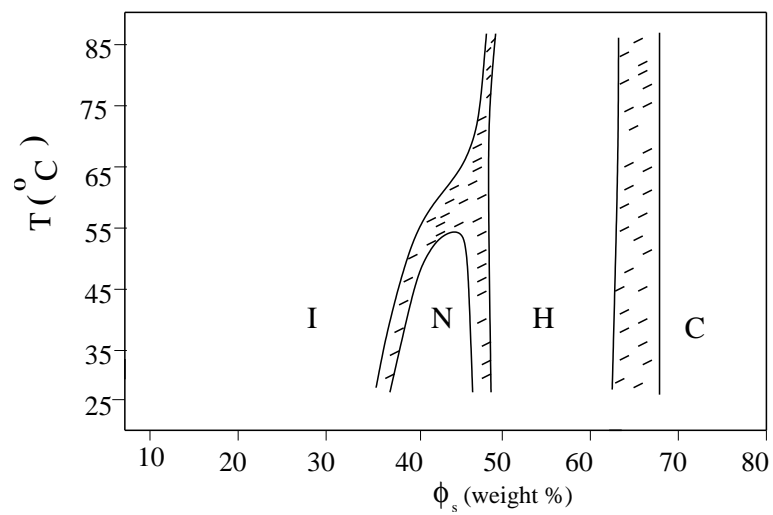


Figure 2.11: Phase diagram of CTAB-SHN-water system at $\alpha = 1.85$. *I*, *N*, *H* and *C* denote the isotropic, nematic, hexagonal and crystalline phases, respectively.



Figure 2.12: Typical thread-like texture of the nematic phase (N) at $\alpha = 1.85$, $\phi_s = 40$ and $T = 30^\circ\text{C}$. The scale bar represents 0.1 mm.

phase is also very viscous and exhibits the characteristic thread-like texture under the polarizing microscope (Fig. 2.12). Pseudo-isotropic regions, where the optic axis is normal to the glass plates, were not found in any of the samples studied. Diffraction patterns of this phase show partial alignment, probably due to the shear flow occurring while the samples were sucked into the capillaries (Fig. 2.13). On increasing ϕ_s the nematic phase transforms into a hexagonal (H) phase, as indicated by the microscopic texture typical of the hexagonal phase. Diffraction patterns of this phase show two peaks in the small angle region with their spacings in the ratio $1:\frac{1}{\sqrt{3}}$ (Fig. 2.14, Table 2.2). A crystalline phase is observed at even higher ϕ_s .

The partial ternary phase diagram at 30°C is presented in figure 2.15. It shows a high degree of symmetry about the line corresponding to equimolar CTAB/SHN composition, as in the case of mixtures of cationic and anionic surfactants.

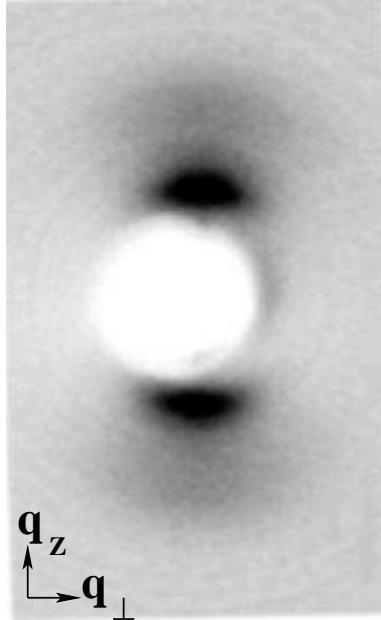


Figure 2.13: X-ray diffraction pattern of the nematic (N) phase at $\alpha = 1.85$, $\phi_s = 40$ and $T = 30^\circ\text{C}$.

ϕ_s	d_1 (nm)	d_2 (nm)	POM	phase
20	very diffuse	-	isotropic	I
40	5.56	-	thread like texture	N
50	5.23	3.02	hexagonal texture	H
60	4.61	2.67	hexagonal texture	H

Table 2.2: Different mesophases in CTAB-SHN-water system at very high SHN concentration ($\alpha = 1.85$).

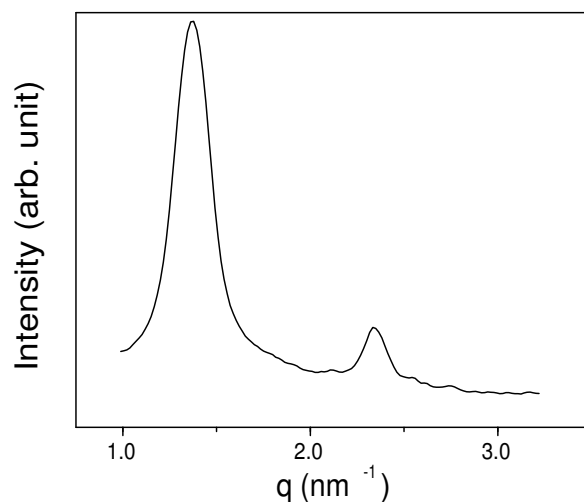


Figure 2.14: X-ray diffraction pattern of the hexagonal phase (H) at $\alpha = 1.85$, $\phi_s = 60$ and $T = 30^\circ\text{C}$.

2.4.2 CTAC-SHN-water system

Phase diagram of the CTAC-SHN-water system has been determined at equimolar composition ($\alpha = 1$) (Fig. 2.16). For $\phi_s < 40$, there is a coexistence of an isotropic and lamellar phases. At higher ϕ_s , a lamellar phase is obtained, which is identified from its oily streak texture and diffraction data. In this system the diffraction pattern of the lamellar phase does not show any diffuse peak in the direction normal to that of the lamellar reflections, indicating the absence of any curvature defects in the plane of the bilayer. It, therefore, is a regular lamellar phase (L_α). In this system the intermediate phase was not observed. Only the regular lamellar phase dominates the phase diagram.

2.4.3 DTAB-SHN-water system

The phase diagram of equimolar mixtures of DTAB and SHN is presented in figure 2.17. For $\phi_s < 45$, the lamellar phase coexists with an isotropic phase. At $\phi_s = 50$, in addition to the lamellar peaks, a diffuse peak indicating the presence of curvature defects in the plane of the bilayer is observed (Table 2.3). The average defect separation decreases on increasing ϕ_s , similar to the trend observed in the random mesh phase of the cesium perfluorooctanoate - water system [20]. The intermediate

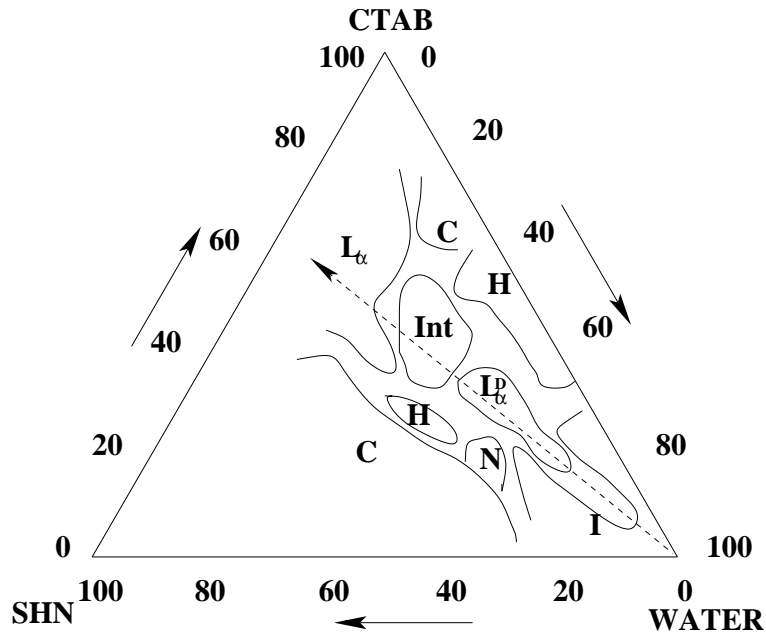


Figure 2.15: Phase diagram of CTAB-SHN-water system at $T = 30\text{ }^{\circ}\text{C}$. The concentrations are in wt%. I , L_{α}^D , L_{α} , H , Int , N and C denote the isotropic, lamellar with curvature defects, regular lamellar phase, hexagonal phase, intermediate phase, nematic phase and crystalline phase, respectively. The dashed line indicates samples with equimolar CTAB/SHN composition.

phase is not observed in this system over the range of ϕ_s and temperature studied.

2.5 Discussion

The high viscosity of the isotropic phase in the CTAB-SHN-water system at low values of α is consistent with the formation of worm-like micelles. This behavior is very similar to that seen in mixtures of CTAB with salts such as KBr, sodium salicylate and sodium tosylate [2, 21, 22]. The growth of these long flexible micelles is attributed to the increase in the end cap energy of the cylindrical CTAB micelles in the presence of these salts.

The observation of a lamellar phase over an extended range of ϕ_s around $\alpha \sim 1.0$ is reminiscent of the behavior of mixtures of cationic and anionic surfactants [6, 7, 8] and also of some mixtures of cationic surfactants and anionic drugs [23]. Although the HN^- counterion is much shorter (length $\sim 5\text{ \AA}$) than the CTAB molecule (length $\sim 17\text{ \AA}$), its incorporation in the CTAB micelle seems to have a similar effect as that of a much longer anionic surfactant. The diffuse peaks in the diffraction patterns of the L_{α}^D phase at lower values of ϕ_s occur in a direction normal

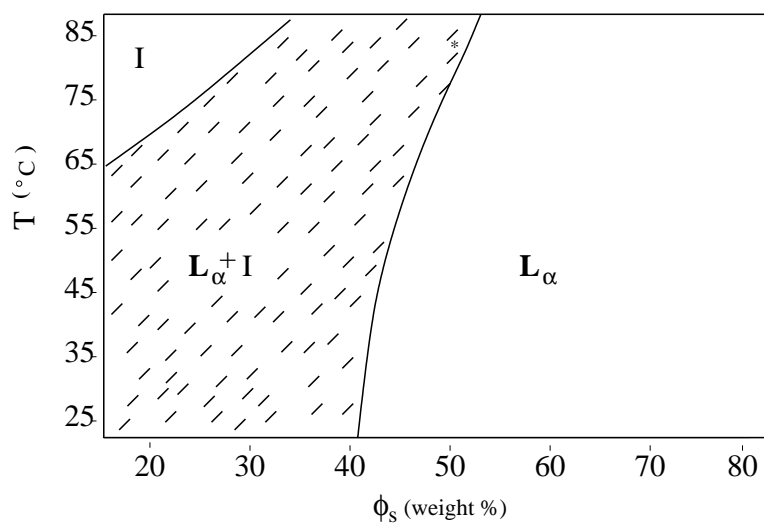


Figure 2.16: Phase diagram of CTAC-SHN-water system at $\alpha = 1.0$. I and L_α denote the isotropic and lamellar phases, respectively.

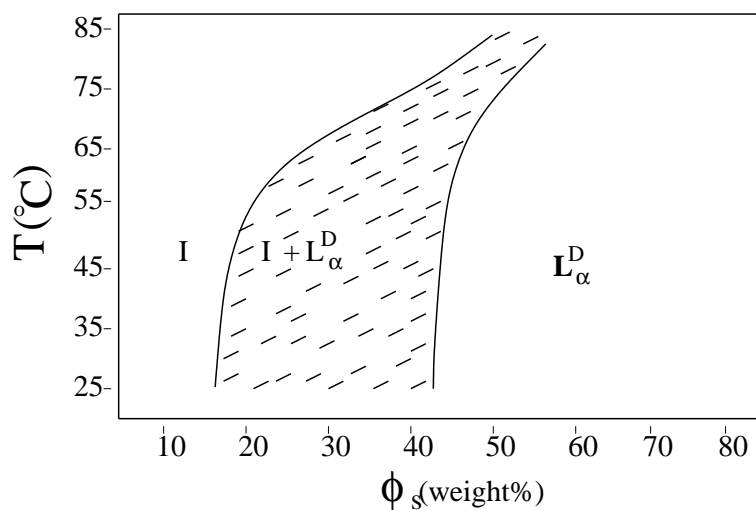


Figure 2.17: Phase diagram of DTAB-SHN-water system at $\alpha = 1.0$. I and L_α^D denote the isotropic phase and lamellar phase with curvature defects.

to the lamellar peaks and can be attributed to positional correlations between defects lying in the plane of the bilayer (Fig. 2.7). Consistent with this picture, the bilayer thickness estimated from the observed lamellar spacing and the surfactant volume fraction is about 10% lower than that obtained at high ϕ_s , when the diffuse peak is absent. Such diffuse reflections have been observed in the lamellar phase of some surfactant systems, such as cesium pentadecafluorooctanoate (CsPFO) [20]. Small angle neutron scattering as well as water diffusion experiments have shown that the diffuse reflections arise from water-filled pores in the bilayer [24]. These defects heal on adding $CsCl_2$ or on increasing the surfactant concentration, to form a lamellar phase without defects. Such curvature defects are also found in some mixed-surfactant systems [25]. Neutron scattering studies on SDS-alcohol-water system have shown that the number of defects per unit area increases as the SDS/alcohol ratio increases. However the pores disappear gradually when the water content is decreased. The existence of similar curvature defects have also been proposed in mixtures of dimyristoylphosphatidylcholine (DMPC) with a shorter chain lipid dihexanoylphosphatidylcholine (DHPC) [26]. The diffraction patterns of this system do not show any diffuse peaks, and the presence of these defects is deduced from the fact that the observed lamellar periodicity is much less than that estimated from the lipid volume fraction. The absence of positional correlations between the defects in this case might be due to the fact that they are quasi-circular pores with no well-defined size. On the other hand, in systems where the diffuse peak is seen it may be better to envisage the bilayers as a mesh-like structure, with ribbon-like segments (Fig. 2.18), rather than as a continuous sheet littered with pore-like defects. Unlike in the CsPFO-water system, the spacing corresponding to the diffuse peak in the present system increases with increasing ϕ_s (Table 2.1). Presently it is not clear if this difference is critical for the occurrence of the intermediate phase in the latter.

The formation of these curvature defects in a mixed surfactant system has been explained in terms of the tendency of one of the surfactant species to aggregate into spherical or cylindrical micelles, both of which have high positive values of mean curvature. The micro environment in the edge of these defects is very similar to that in the micelles, and hence their formation helps to reduce the overall energy of the system [27]. A single ionic surfactant can also mimic a two

Table 2.3: Variation of the lamellar periodicity (d) and the average in-plane periodicity (d_d) in the DTAB-SHN-water system at $\alpha = 1$ and $T = 30$ °C.

ϕ_s	$d(\text{nm})$	$d_d(\text{nm})$	POM	phase
60	4.38	5.87	oily streak texture	L_α^D
70	3.81	5.23	oily streak texture	L_α^D
80	3.54	4.42	oily streak texture	L_α^D

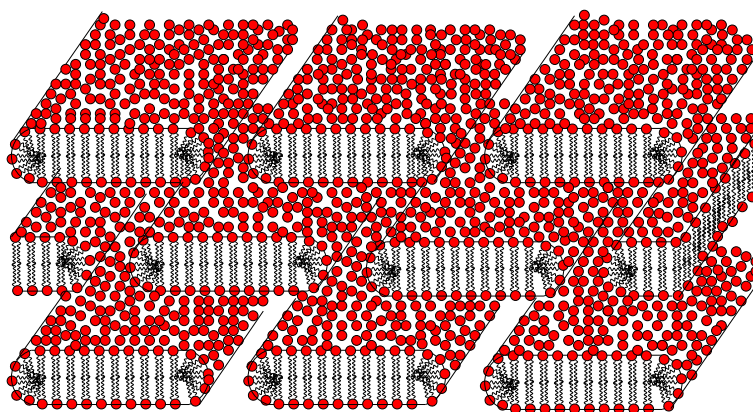


Figure 2.18: Schematic diagram of lamellar phase made up of ribbon like segments. Note, however, that ribbons in adjacent layers need not be oriented in the same direction.

[NaBr]	$d(\text{nm})$
0.00	4.71
0.12	4.79
0.25	5.16
0.50	5.67
1.00	6.10

Table 2.4: Variation of the lamellar periodicity (d) at $\alpha = 1.0$ and $\phi_s = 10$ with added NaBr salt at $T = 30^\circ\text{C}$.

component system by having a higher degree of ionization near the edges of these defects. In the present case it is very likely that the CTAB concentration is higher near the defect edges, reflecting the preference of CTAB to form cylindrical micelles. The curvature defects in the lamellar phase gradually disappear on decreasing the water content at high temperatures. However, at lower temperatures an intermediate phase occurs in between the two lamellar structures. This phase is found over a very broad composition range. The detailed analysis of the structure of this phase is described in the next chapter.

In equimolar mixtures, the lamellar phase coexists with an isotropic phase up to $\phi_s \sim 30$, beyond which a pure lamellar phase is found. Interestingly, the lamellar periodicity (d) increases with increasing ϕ_s in the coexistence region and then decreases in the lamellar phase (Table 2.1). Whereas the decrease at higher ϕ_s can be attributed to the volume constraint as usual, the observed increase at lower ϕ is somewhat surprising. One possible cause of this behavior is the increase in the concentration of Na^+ and Br^- ions in the solution, which are released from the two components. In order to check this possibility we have measured the influence of added NaBr on the lamellar periodicity at a lower value of ϕ_s (Table 2.4). The maximum value of added salt corresponds to the expected salt concentration in the solution at ϕ_s corresponding to the maximum in d . From the table it is clear that this salt can not solely explain the observed swelling with ϕ_s . The additional contribution might come from the osmotic pressure exerted by the isotropic phase which could be a micellar solution. In order to explain the observations the osmotic pressure should decrease with increasing ϕ_s , along with the relative amount of the isotropic phase. Further studies are necessary to test these possibilities.

On increasing α to 1.85 the lamellar phase disappears and the phase behavior is somewhat analogous to that at very low values of α . A similar behavior is also seen in other mixtures of CTAB with strongly bound hydrophobic counterions, and is usually attributed to the fact that the aggregates at these compositions are highly charged, as those at very low counterion concentration. The only difference is the observation of the nematic phase at $\alpha = 1.85$. In this connection it should be noted that a nematic phase made up of rod-like micelles has been reported in the CTAB-water system from 26 to 30 wt.% CTAB concentration, below 42 °C [11]. However, we did not observe this phase even at the lowest α studied. The nematic phase seems to be suppressed by SHN at these compositions, although at much higher values of α this phase reappears. The flow alignment of the nematic phase, observed in the diffraction experiments, and the absence of pseudo-isotropic regions in its microscope texture suggest that it is made up of linear surfactant aggregates. The high viscosity of this phase indicates that these are long worm-like micelles, and not shorter rod-like ones proposed in the N phase of the binary CTAB-water system.

The overall symmetry of the ternary phase diagram about the equimolar composition of the two species is very similar to that observed in the case of mixtures of cationic and anionic surfactants.

On the addition of strongly bound counterion, both CTAC and DTAB show only the lamellar phase over wide range of concentration. The intermediate phases of CTAC-water binary system and the bicontinuous cubic phase in case of DTAB-water system disappear. With the change of counterions, it is found that the CTAC-SHN system does not show defects in the lamellar phase. It has been reported that the effective binding of Br^- ions to the surfactant bilayers is much higher than that of Cl^- ions [28]. Even for neutral lipid bilayer a similar behavior has been observed. In case of CTAB the formation of defects is explained above in terms of partial dissociation of the Br^- counterions. In case of CTAC, on the other hand, the dissociation is expected to be almost complete. Therefore, the system would prefer to form continuous bilayers, where the microenvironment of all the molecules is the same. This might explain the absence of curvature defects in this system.

On decreasing the chain length, it is found that although the DTAB-SHN system forms curvature defects, the average defects separation decreases with surfactant concentration. The appear-

ance of defects can be again explained by the binding of Br^- ions on the bilayer. The decrease of defect separation and their effect in forming the intermediate phase will be discussed in the next chapter.

2.6 Conclusion

A partial phase diagram of the CTAB-SHN-water system has been constructed from optical microscopy and x-ray diffraction studies. A variety of phases, such as hexagonal, lamellar with curvature defects, intermediate, regular lamellar and nematic, have been identified. The phase behavior is found to be fairly symmetric about the equimolar CTAB-SHN composition, as seen in mixtures of cationic and anionic surfactants. The curvature defects, present in the L_{α}^D phase at higher water content, are gradually annealed on decreasing the water content at high temperatures. However, at lower temperatures this occurs across an intermediate phase, which consists of an ordered array of such defects and is the subject of the next chapter. Replacing the bromide ion by chloride ion removes the curvature defects, which indicates the ion specificity for such structure formation. Although the shorter chain surfactant is able to produce the curvature defects, this system is unable to induce their correlated three-dimensional structure.

Bibliography

- [1] H. Rehage and H. Hoffmann *J. Phys. Chem*, **92**, 4712 (1988).
- [2] T. Shikata, H. Hirata and T. Kotaka *Langmuir*, **4**, 354 (1988).
- [3] M. E. Cates and S. J. Candau *J. Phys: Condens. Matter*, **2**, 6869 (1990).
- [4] J. F. Beret *Cond-mat/0406681* (2004).
- [5] E. H. Lucassen-Reynders, J. Lucassen and D. Giles *J. Colloid Interface Sci.* **81**, 150 (1981).
- [6] E. W. Kaler, K. L. Herrington, A. K. Murthy and J. A. N. Zasadzinski, *J. Phys. chem.* **96**, 6698 (1992).
- [7] M. T. Yacilla, K. L. Herrington, L. L. Brasher, and E. W. Kaler *J. Phys. Chem.* **100**, 5874 (1996).
- [8] K. L. Herrington, E. W. Kaler, D. D. Millar, J. A. Zasadzinski and S. Chiruvolu *J. Phys Chem.* **97**, 13792 (1993).
- [9] M. J. Blandamer, B. Briggs, P. M. Cullis and B. F. N. Engberts *Phys. Chem. Chem. Phys.* **2**, 5146 (2000).
- [10] X. Auvray, C. Petipas, R. Anthore, I. Ricco and A. Lattes *J. Phys. Chem.* **93**, 7458 (1989).
- [11] L. Coppola, R. Gianferri, I. Nicotera, C. Oliviero and G. A. Ranieri *Phys. Chem. Chem. Phys.* **6**, 2364 (2004).
- [12] B. K. Mishra, S. D. Samant, P. Pradhan, S. B. Mishra and C. Manohar *Langmuir* **9**, 894 (1993) .

- [13] K. Horbaschek, H. Hoffmann and C. Thunig *J. Colloid Interface Sci.* **206**, 439 (1998)
- [14] R. A. Salkar, P. A. Hassan, S. D. Samant, B. Valaulikar, V. V. Kumar, F. Kern, S. J. Candau and C. Manohar, *Chem. Commun.* **10**, 1223 (1996).
- [15] E. Mendes, J. Narayanan, R. Oda, F. Kern, S. J. Candau and C. Manohar *J. Phys. Chem. B.* **10**, 2256(1997)
- [16] E. Mendes, R. Oda, C. Manohar and J. Narayanan *J. Phys. Chem.* **102**, 338 (1998).
- [17] R. Krishnaswamy, Ph. D Thesis: *Structure of Surfactant-Polyelectrolyte Complexes*, Jawaharlal Nehru University, New Delhi (2003).
- [18] U. Henriksson, E. S. Blackmore, G. J. T. Tiddy and O. Soderman *J. Phys. Chem* **96**, 3894 (1992).
- [19] K. M. McGrath *Langmuir* **11**, 1835 (1995).
- [20] M. S. Lever and M. C. Holmes *J. Phys. II France* **3**, 105 (1993).
- [21] A. Khatory, F. Lequeux, F. Kern and S. J. Candau, *Langmuir* **9**, 1456 (1993).
- [22] V. Hartmann and R. Cressely *J. Phys II France* **7**, 1087 (1997).
- [23] T. Bramer, M. Paulsson, K. Edwards and K. Edsman *Pharmaceutical Research* **20**, 1661 (2003).
- [24] M. C. Holmes, P. Sotta, Y. Hendrikx and B. Deloche *J. Phys. II France* **3**, 1735 (1993)
- [25] Y. Hendrikx, J. Charvolin, P. Kekicheff and M. Roth *Liq. Cryst.* **2**, 677 (1987).
- [26] M. Nieh, C. J. Glinka, S. Kroeger, R. S. Prosser and J. Katsaras *Langmuir* **17**, 2629 (2001).
- [27] C. K. Bagdassarian, D. Roux, A. Benshaul, and W. M. Gelbert *J. Chem. Phys.* **94**, 3030 (1991).
- [28] H. N. Patrick and G. G. Warr *J. Phys. Chem.* **100**, 16268 (1996).